ISSN 1061-8309, Russian Journal of Nondestructive Testing, 2020, Vol. 56, No. 11, pp. 936–947. © Pleiades Publishing, Ltd., 2020.

RADIO WAVE METHODS

Forward Simulation Signal of Underground Pipeline Based on Ground Penetrating Radar

Lei Gao[a], *, Yi Luo, Hantao Song[a], Gangqiang Kong[a], and Guohui Hu[a]

[a]*Key Laboratory of Ministry of Education for Geomechanics and Embankment Engineering, Hohai University, Nanjing, Jiangsu, 210098 China*

**e-mail: gaoleihhu@hhu.edu.cn*

Received January 2, 2020; revised February 20, 2020; accepted September 11, 2020

Abstract—The ground penetrating radar was applied to the detection of underground pipeline. The signal of ground penetrating radar was analyzed to simulate the different sizes of pipelines and oil. The data were processed by GRED HD software. Radar profiles and single-channel waveforms of underground pipelines and oil were obtained. The nonstationary signals of geological radars were processed and analyzed by the finite-difference time-domain method. The different radar characteristic signals of underground pipelines and radar signal variations of pipeline oil were discussed. It can improve the accuracy of interpretation of underground pipelines and oil.

Keywords: underground pipeline, ground penetrating radar, finite difference in time domain, forward simulation signal

DOI: 10.1134/S1061830920110042

1. INTRODUCTION

In recent years, the economic construction has achieved remarkable development in China. With the rapid urbanization, the distribution of underground pipeline as urban lifeline becomes more and more complicated. Most cities have not yet established a complete underground pipeline network management system. The engineering accidents caused by construction or underground pipelines excavation frequently occur in the construction process, the underground pipelines are often aging or even broken. The problem of soil pollution caused by oil from pipeline is particularly prominent, which affects the progress of construction seriously [1]. It is important to find an effective method to detect underground pipelines and oil from pipeline, it will provide a basis for pipeline detection. At present, the common methods are based on feedback information to trace the governance, the condition of inspection pipeline are randomly and even require the excavation of ground. The operation is cumbersome, it is difficult to find pipeline hazards due to the limited testing range. The ground penetrating radar (GPR) is a new type of underground target finding method. It has outstanding features such as high precision, good continuity and small disturbance [2, 3]. It can meet the requirement of finding underground pipelines and leakage oil well [4, 5]. The GPR transmits high-frequency electromagnetic waves through the transmitting antenna, it infers the spatial position and shape distribution of different media through information such as the waveform, amplitude and phase of reflected electromagnetic waves received by the receiving antenna. The detectors mainly rely on the analysis of strong reflection in-phase axis of the geological radar profile to infer the underground pipeline and the leakage oil. The complex detection results are very dependent on the experience of detector, which can easily lead to misjudgment and oil from underground pipelines. Tst Amran et al. conducted a series of laboratory experiments using 800-MHz antenna, the GPR performance on detecting underground pipeline and locating water leakage were investigated and validated [6]. Varughese A. et al. applied the GPR for solution, when other conventional investigations cannot work in hydroelectric projects and in the detection of utilities well [7]. Ó. PueyoAnchuela et al. used GPR to evaluate the seepage endangers of dam integrity with different antennas, and the data were integrated with infrared thermo graphic images [8]. Chen Jun and other experts initially applied geological radar to urban underground pipeline detection [9, 10]. At present, GPR has been widely used and studied in the engineering field, but the researches mainly focus on tunnel advance prediction [11], lining defect detection [12], bridge and road quality disease detection [13, 14], there are few studies about the application of geological radars in the inversion of underground pipelines,

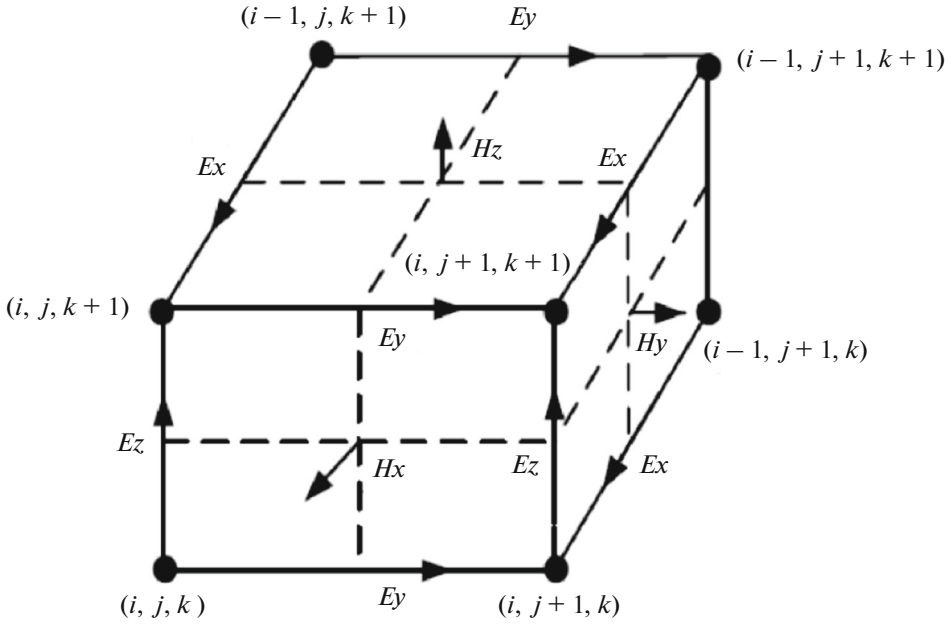

Fig. 1. Schematic diagram of Yee cell [15].

especially the systematic research on the in-depth analysis of the location, size, and filling characteristics of underground pipelines and geological radar image signals.

In this paper, a physical simulation model is established for different scenarios such as a single pipeline, different size pipelines and pipeline filled oil. Two-dimensional geological radar detection and forward modeling are carried out on different models of underground pipelines through GPRMax program and MATLAB software programming. According to the special conditions of different pipe diameters and oil, the underground pipelines and features were quantitatively identified by spectrum analysis, the basic principles of geological radar detection signals analysis of different characteristics of underground pipelines were summarized.

2. GPR FORWARD MODELING METHOD

2.1. Principle of Time Domain Finite Difference Method Forward

The high-frequency electromagnetic waves of geological radar are directed into the ground through the transmitting antenna, they are returned to the ground after being reflected by the underground formation or cavity with electrical differences and then received by the receiving antenna. When the high frequency electromagnetic waves propagate in the medium, the propagation path, electromagnetic field strength, waveform variation with the electrical characteristics and geometry of the medium are tested. The spatial location and structure of the subsurface interface or geological body can be determined by collecting time domain waveforms, processing and analysis.

The finite difference time domain (FDTD) method is a numerical solution of Maxwell's equations proposed by Kane Yee in 1966. It can calculate electromagnetic wave values and simulate the propagation of electromagnetic waves in underground media during geological radar detection. It takes the Yee cell as a discrete unit and divides the entire simulation space into a grid composed of Yee cells. Each cell has its own electromagnetic field component, as shown in Fig. 1.

In two-dimensional space, the rotation of the cell in the x-axis direction is:

$$\left.\begin{aligned} \frac{\partial E_x}{\partial z} - \frac{\partial E_z}{\partial x} &= -\mu \frac{\partial H_y}{\partial t} \\ \frac{\partial H_x}{\partial z} - \frac{\partial H_z}{\partial x} &= \varepsilon \frac{\partial E_y}{\partial t} + \sigma E_y \end{aligned}\right\}. \tag{1}$$

Record the observation node $E_x(x, y, z)$ coordinates are $(i + 1/2, j, k)$, Remember the moment $t = (n + 1/2)\Delta t$. When calculating the electromagnetic field variables in the Yee cell, it is often discrete at equal intervals, i.e.:

$$\Delta x = \Delta y = \Delta z = \delta. \tag{2}$$

The FDTD time update equation [16] for electric and magnetic fields in space can be simplified as:

$$\begin{aligned} E_x^{n+1}(i+1/2, j, k) &= CA(m)gE_x^n(i+1/2, j, k) + CB(m)[H_z^{n+1/2}(i+1/2, j+1/2, k) \\ &- H_z^{n+1/2}(i+1/2, j-1/2, k) - H_y^{n+1/2}(i+1/2, j, k+1/2) + H_y^{n+1/2}(i+1/2, j, k-1/2)]. \end{aligned} \tag{3}$$

In the formula, $CA(m) = \dfrac{1 - \dfrac{\sigma(m)\Delta t}{2\varepsilon(m)}}{1 + \dfrac{\sigma(m)\Delta t}{2\varepsilon(m)}}$, $CB(m) = \dfrac{\dfrac{\Delta t}{\varepsilon_0 \delta}}{\varepsilon_r(m) + \dfrac{\sigma(m)\Delta t}{2\varepsilon_0}}$, m, the values are in order $(i, j + 1/2, k + 1/2)$.

$$\begin{aligned} E_x^{n+1}(i, j+1/2, k+1/2) &= H_x^{n-1/2}(i, j+1/2, k+1/2) + CP(m)[E_y^n(i, j+1/2, k+1) \\ &- E_y^n(i, j+1/2, k) - E_z^n(i, j+1, k+1/2) + E_z^n(i, j, k+1/2)]. \end{aligned} \tag{4}$$

In the formula, $CP(m) = \dfrac{1 - \dfrac{\sigma_m(m)\Delta t}{2\mu(m)}}{1 + \dfrac{\sigma_m(m)\Delta t}{2\mu(m)}} CQ(m) = \dfrac{\dfrac{\Delta t}{\mu(m)}}{1 + \dfrac{\sigma_m(m)\Delta t}{2\mu(m)}}$, m, the values are in order $(i, j + 1/2, k + 1/2)$.

The above Eqs. (3) and (4) describe the propagation process of a similar longitudinal wave from the coordinate axis x direction, and the formulas are the same in both the *y* and *z* directions. The amount of cellular electromagnetic field depends on adjacent cellular transmission. The component value on the grid point inside the cell depends on the magnitude of point in the previous time step and the value of other point in the adjacent point half the time step. According to Eqs. (3) and (4), the electromagnetic field can be alternately calculated on the analog region cells one by one, the numerical simulation results can be obtained after all the preset time steps are performed. The FDTD method can be quickly iteratively calculated by computer, it has good stability and convergence. It has become the main method for numerical calculation of electromagnetic fields.

The finite-difference time-domain method is an approximate calculation of the Maxwell's curl equation, when the computer performs numerical simulation, the nondispersive medium is discretely processed, resulting in dispersion. In order to satisfy the dispersion condition, the wavelength needs to be greater than or equal to 12 or more calculation grids. At the same time, it should ensure the stability of Maxwell's equations, the time step and space grid step size must satisfy the following relationship [17]:

$$\Delta t \le \frac{1}{c\sqrt{\dfrac{1}{(\Delta x)^2} + \dfrac{1}{(\Delta y)^2} + \dfrac{1}{(\Delta z)^2}}}. \tag{5}$$

2.2. Gprmax Forward Modeling Method

The GPRMax program used in the numerical simulation is a geological radar forward modeling program developed on the basis of the finite-difference time-domain method. It was first designed by Antonis Giannopoulos in 1996. It uses the Yee grid algorithm to solve the Maxwellian group, mainly used in the field of geological radar, it can be simulated in other electromagnetic wave propagation.

GPRMax is a geological radar forward modeling program based on the finite difference time domain method. The stratum structure layer is constructed in an input file with a suffix of .in, and the code is input to set physical parameters, electromagnetic parameters and simulation parameters of each structural layer. After computer simulation, the model output file with the suffix.out and the waveform data output file with the suffix.geo are obtained. Then the program is written in MATLAB software to read the output file and process the data to obtain the geological radar forward simulation image.

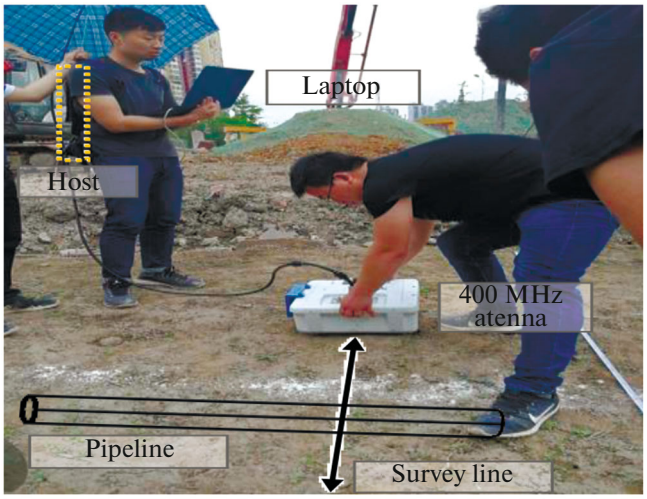

Fig. 2. Photo of pipeline site detection.

3. FORWARD MODELING OF UNDERGROUND PIPELINE

3.1. Stratum Model Establishment and Parameter Setting

From the project in the Hexi area of Nanjing city, China, it was found that there was a pipeline buried in the ground. In order to detect the distribution of pipelines and prevent engineering accidents, the geological radar detection was carried out. In the construction site, 10 lines are arranged parallel, the Italian IDS RIS type geological radar was used together with the 400 MHz and 1600 MHz radar antenna. The photo is shown in Fig. 2.

According to the actual soil structure of the project, a 1 m (y-axis depth) × 2 m (x-axis antenna scanning distance) formation model is established, which is divided into three layers. The first layer is a 0.1 m thick plain concrete layer, the second layer is a 0.4 m thick miscellaneous fill soil layer, the third layer is a 0.5 m thick clay base layer, and the PVC line is located in the miscellaneous soil layer. The relative dielectric constant and conductivity of the medium were obtained by relevant data [18]. The summary of forward modeling parameters is shown in Table 1.

The transceiver antenna is located on a horizontal line 2.5 mm above the air-soil interface. The structural excitation source is set to the Ricker wave closest to the electromagnetic wave of the geological radar transmitting antenna, and the model boundary is set to the PML boundary condition.

3.2. Forward Modeling of Different Sizes of Pipelines

According to the stratigraphic model constructed in the previous section, a separate circular pipeline is placed in the soil base. The soil layer structure model is unchanged. The surface depths of different sizes pipes are the same with 0.29 m and circular. The diameters are 0.08, 0.12, and 0.16 m respectively. Other simulation parameters are consistent with the previous one, and the model structure is shown in Fig. 3.

Table 1. Forward modeling parameters

Parameter Type	Numerical value	Parameter type	Relative permittivity ε_r	Conductivity σ, S/m
Type of incentive source	Ricker wave	Air	1	0
Excitation source frequency, MHz	1600	PVC pipeline	3	10^{-3}
Space grid step size, m	0.002 × 0.002	Oil stain	75	10^{-2}
Antenna step size, m	0.02	Sand	6	10^{-5}
Electromagnetic wave velocity, cm ns^{-1}	5	Miscellaneous fill	8	10^{-3}
Time window, ns	20	Clay	12	10^{-1}

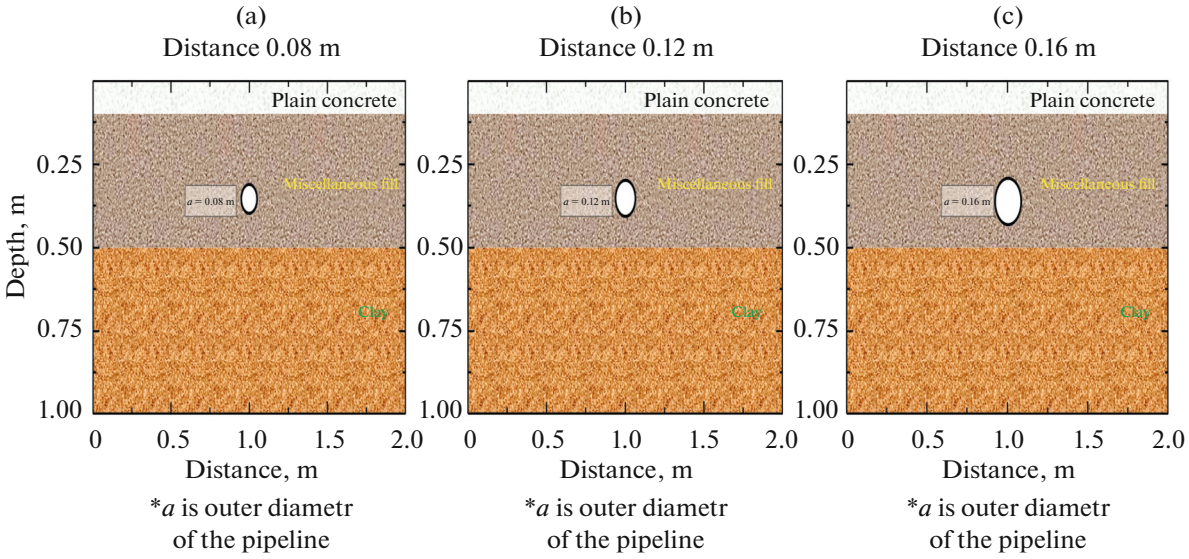

Fig. 3. Different size pipeline models.

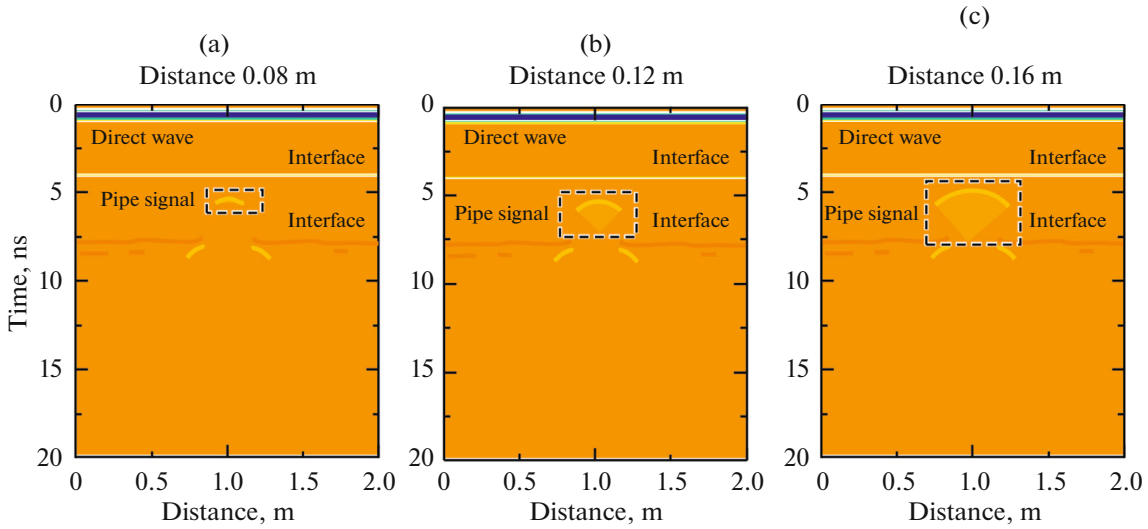

Fig. 4. Forward simulations of different size pipes.

The forward simulation results are shown in Fig. 4. The interface signal is consistent with the previous simulation results. From Figs. 4a to 4c, it can be found that the signal on the radar image is clearer when the radius of circular pipe is larger. In addition, the radius of the hyperbola curvature is larger, the hyperbola extends to the longer both ends, the top of hyperbolic curve is larger. The difference between the x-axis coordinate values at both ends of the pipe signal hyperbola does not match the actual diameter of the pipe, and the diameter of the pipe area cannot be directly obtained.

Table 2 shows that the pipeline size and depth can be quantitatively identified within certain accuracy.

3.3. Forward Modeling of Single Pipeline Positioning

The distance between the center of the pipeline area and road surface is 0.35 m. Considering the material of the site, the material of pipe is set to PVC and the dielectric constant is set to 8. The center coordinates of the pipe area are (1.0, 0.35) and the pipe diameter is 0.12 m. In the *y*-axis direction of 0.6 ns is the direct wave formed by the electromagnetic wave propagating in the air. At 4.2 ns, the boundary signal

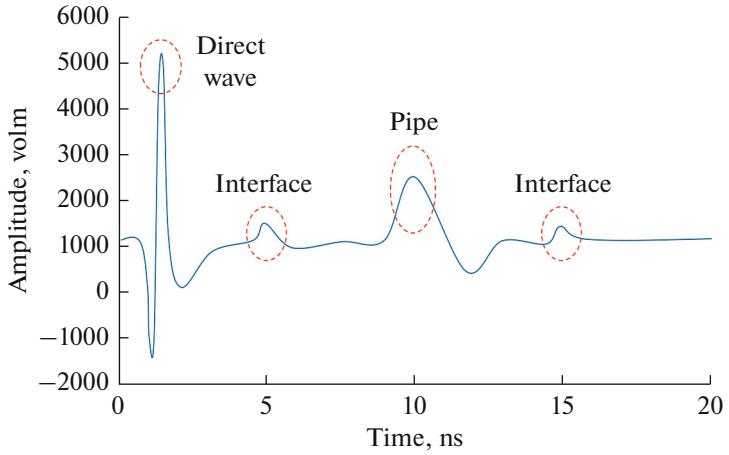

Fig. 5. Single channel wave waveform of a single pipe.

between the plain concrete surface layer and the miscellaneous filling layer is at 8 ns, the interface signal between the mixed filling layer and the clay base layer is 8 ns. In the clay base layer, the circular underground pipeline exhibits a hyperbolic characteristic signal with the curved opening facing down when time is between 4.2 and 8 ns. The ratio of the *y*-axis coordinate value to the *y*-axis coordinate difference of the two interface signals is 0.46. In the model, the difference between the upper surface of the pipeline area and the clay base layer is 0.43, the ratio between the two is relatively close. The horizontal center position and the upper surface depth of pipeline can be calculated from the vertex coordinate values of the hyperbola on the radar image, the depth of lower surface for the pipeline is difficult to calculate directly. The single-channel waveform of pipeline is extracted, which can be shown in Fig. 5.

A partial enlarged view is shown in Fig. 6. Electromagnetic waves are reflected at the interface of the medium, the vibrations are generated on the single-channel waveform. The amplitude of the direct wave is large, and the amplitude is greatly attenuated after entering the underground. Compared with the radar image, the electromagnetic wave in the single-channel waveform has a waveform vibration when it passes through the lower surface of the pipe region. The vertical depth of the pipe can be obtained according to the time and wave velocity of the electromagnetic wave propagating in the pipe region. The horizontal signals of upper and lower surfaces for electromagnetic wave passing through the pipeline area are 5.4 and 6.6 ns, respectively. The one-way travel time is half of the differences coordinate values, and the domain wave velocity is 21.2 cm/ns. The vertical depth of the pipe is 12.72 cm, which is close to the actual vertical depth of 12 cm for model. The results show that this quantitative analysis is feasible and accurate.

3.4. Forward Modeling of Different Filling Pipeline

In order to analyze the influence of different fillers on the pipeline, two scenarios are set. Two different sizes of pipelines are set in each scenario, the electromagnetic wave reflection characteristics of the pipeline filled with different fillers are highlighted by comparing the results of two pipeline simulations. The

Table 2. Comparison of setting conditions and simulation result data

Number	Actual pipe characteristics		Pipe feature read by simulation results		Average relative error of pipe diameter $\overline{\delta}_1 = 8\%$
	pipe diameter, cm	pipe depth, cm	pipe diameter, cm	pipe depth, cm	
1	8	25	9	26	
2	8	25	7	24	
3	12	25	13	27	Pipeline depth average relative error $\overline{\delta}_2 = 6\%$
4	12	25	11	28	
5	16	25	17	25	
6	16	25	16	25	

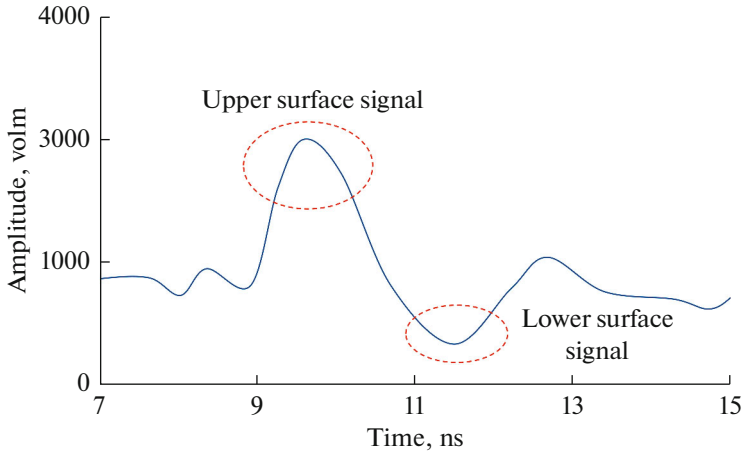

Fig. 6. Partial enlarged view of the single channel waveform of a single pipe.

pipeline filling media in the two scenarios are: scenario (1) assumes that the filling in the pipeline is air, and scenario (2) assumes that the filler in pipeline is oil. The specific media parameters are shown in Table 3. Through the comparison of the simulation data of the front and back groups, it is used to explain the influence of the different fillers inside the pipeline on the electromagnetic wave propagation.

The size of the soil layer is expanded to 4 m in length and 1 m in depth. The pipeline is still set in the miscellaneous soil layer. The distance between the centers of two pipelines is 0.35 m from the road surface. The material of pipe is set to PVC and the dielectric constant is set to 8. The coordinates of the center of pipelines are (0.5, 0.35) and (1.5, 0.35). Other simulation parameters are same, and the model structure is shown in Fig. 7.

The simulation is performed by using GPRMax2d, the radar profile in the simulation scenario (1) is shown in Fig. 8. The relative dielectric constant of the pipeline is set small, mainly for the simulation study of the pipeline when it is free of oil. Due to the small extent of pipeline, the pipeline 1 only shows a hyperbolic reflection signal with a small curvature on the radar profile, the excitation wave is more excited, the hyperbolic boundary propagates farther on the radar profile. It shows that when the pipeline is gradually reduced to a certain extent, the geological radar loses its ability to judge the scope of the pipeline. For the two pipes, the pipe signal shows an asymmetrical feature in the profile. This is mainly the result of the difference between the medium in the pipeline and the surrounding medium. There is a certain degree of electromagnetic wave loss in the process of electromagnetic signal propagating from the top to the bottom.

Two single-channel waves are extracted as shown in Fig. 9.

For both pipelines, there are obvious reflection anomalies in the radar single-channel wave diagram. It depends on the size of the pipe, the reflection shows a different performance. There is a diffraction phenomenon of electromagnetic waves at the boundary of the pipeline. This is a concrete manifestation of the electrical difference between the pipeline and surrounding medium. The approximate area of pipeline can be judged by the position of boundary diffraction. The electromagnetic wave signal and diffraction signal of boundary are superimposed at the bottom to form a type hyperbolic intersection, the bottom of pipe can be judged by the position of intersection. The single-wave can distinguish the first arrival wave at the top of pipeline. The medium in the pipeline is a high-resistance medium relative to the surrounding medium, the first arrival reflected wave is in the same direction as the incident wave. Theoretically, the phase of the reflected wave signal at the bottom of pipe should be opposite to the incident wave. Due to

Table 3. Pipe and filling media parameters

Case	Diameter, cm	Relative permittivity	Conductivity, S m^{-1}
Pipe one	12	8	0.1
Pipe two	20	8	0.1
Air	–	1	0
Oil	–	70	0.01

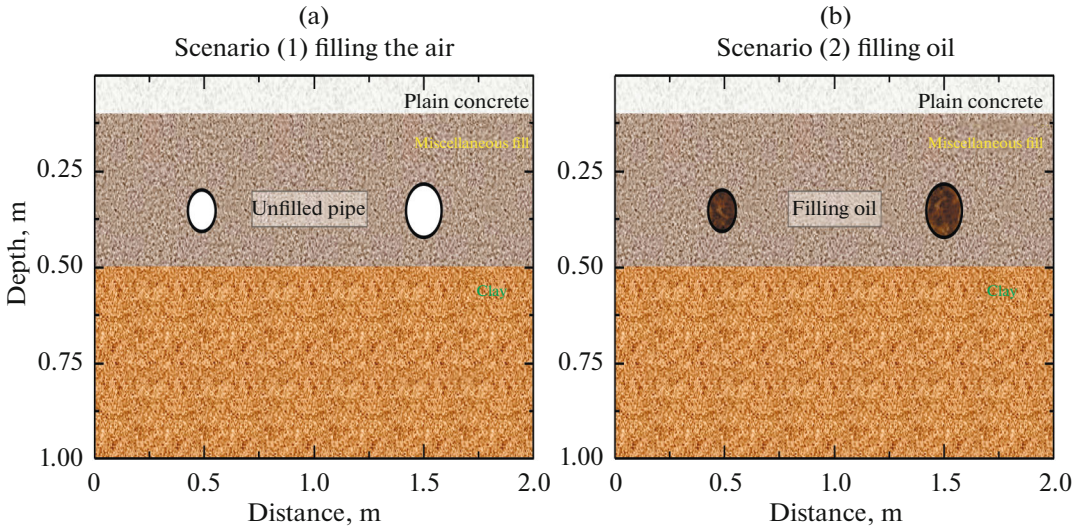

Fig. 7. Different filler models in the pipe.

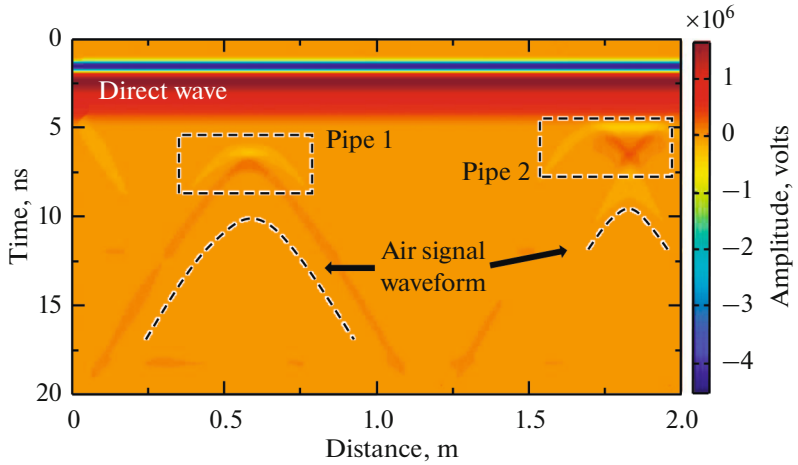

Fig. 8. Pipeline filled air numerical simulation radar profile.

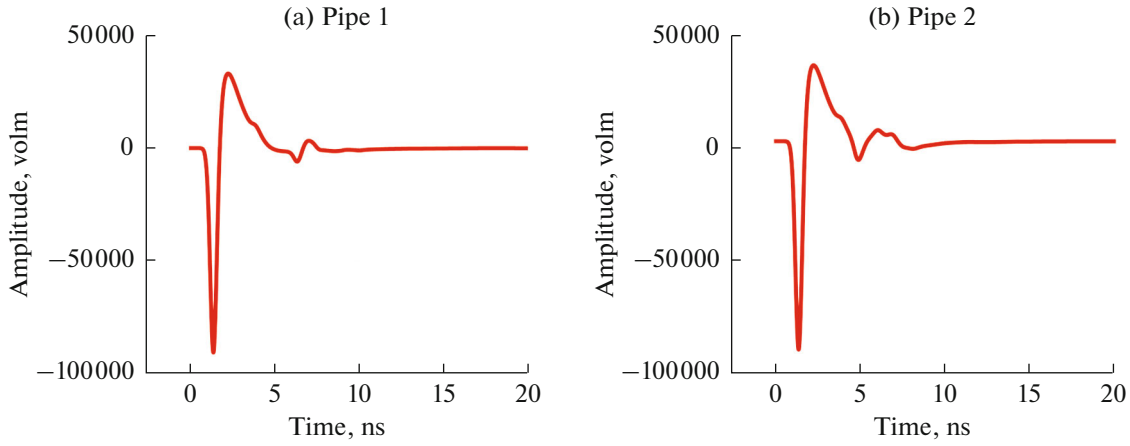

Fig. 9. Pipeline filled air numerical simulation radar single channel diagram.

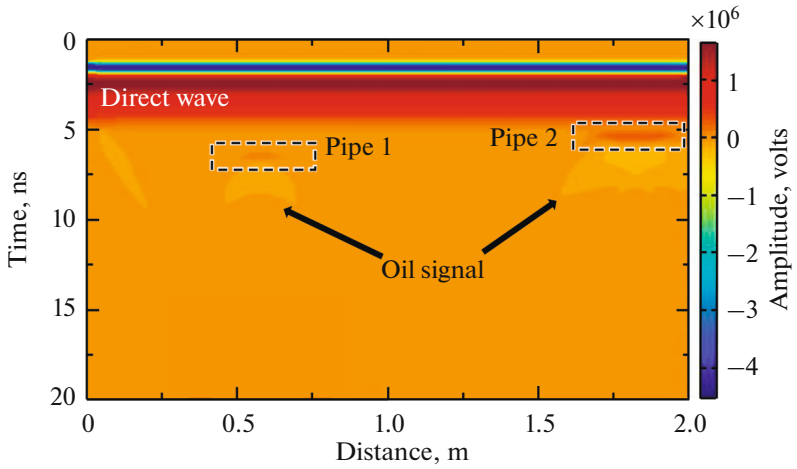

Fig. 10. Pipeline fill oil numerical simulation radar profile.

the superposition of the reflected wave delay at the top of pipe and the initial wave at the bottom, there is no obvious phase inflection point signal at the initial wave position of the pipe. In addition, the absorption of the electromagnetic wave amplitude is more obvious when the pipe diameter is larger.

The radar profile in the simulation scenario (2) is shown in Fig. 10 (Here, the actual time window of the model is 19.9 ns instead of 20 ns to eliminate the interference signal of the bottom part.). The relative dielectric constant of the air is set to 81, the electromagnetic wave characteristic of the simulated pipeline filled with oil can be seen. The two pipeline areas have strong reflection, but the reflection area is small, the absorption of electromagnetic waves is strong without unnecessary diffraction. The difference between the pipe and surrounding medium is large, the body shape is small, there are multiple wave reflections under it. The second range of the pipeline is large, the electromagnetic wave propagates for a certain distance. The rain-like high-resistance medium is equivalent to a high-frequency filter. The lower part is a low-frequency signal with a large wavelength, the effective signal is less. The greater difference between the electrical parameters of filling medium in the pipeline and surrounding medium are shown, the stronger signal reflection are the more obvious characteristics.

For a single channel signal, as shown in Fig. 11, the material filled in the pipe can be judged by the phase change. For the case of oil, the single pass wave in Fig. 11 exhibits a phase reversal characteristic at the reflection of the pipe. In Fig. 9, the single-channel wave exhibits a feature in which the amplitude in the same direction becomes large. In contrast to scenario (1) and scenario (2) in the oil-filled state, the electromagnetic wave propagation velocity becomes slower, the single-channel wavelength becomes significantly larger, the amplitude absorption effect is more obvious. In the air-filled state, there are more high-frequency signals. The electrical difference between the filling medium in the pipe and surrounding medium is larger, the reflection is more obvious and strong. In the single-channel waveform diagram, since the pipeline with oil is a high-resistance medium, the first-coming emission wave at the top of the pipeline is opposite to the phase of the incident wave. The bottom first arrival reflected wave and the top reflected wave show interference stacking, the inflection point is submerged in the signal.

The size of the oil-filled area is difficult to judge from the range of reflected wave at the pipe position, but the size of the lower-direction off-axis is proportional to the pipe size. The single-wave can distinguish the first arrival wave at the top of pipeline. The medium in the pipeline is a low-resistance medium with respect to the surrounding medium, the first arrival reflected wave is in the same direction as the incident wave. The phase of reflected wave signal at the bottom of contaminated soil should be opposite to the incident wave. Due to the superposition of the top reflected wave delay of the oil area and the initial reflection of the bottom, there is no obvious phase inflection point signal at the beginning of the pipeline. In addition, the absorption of the electromagnetic wave amplitude is relatively large.

Compared with the pipe one, the distance between the parallel multiple reflections of the pipe two is larger. It is difficult to judge the bottom of void from the original signal. In addition, there is a multi-wave reflection signal with large amplitude at the bottom of single-channel signal, there is a certain offset phenomenon between the single-wave tail signal and the center position.

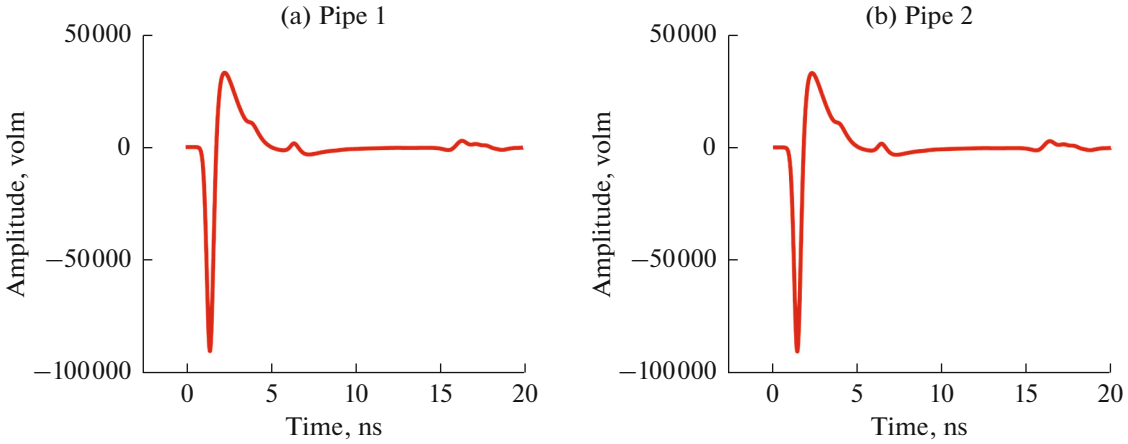

Fig. 11. Pipeline filling oil numerical simulation radar single channel wave.

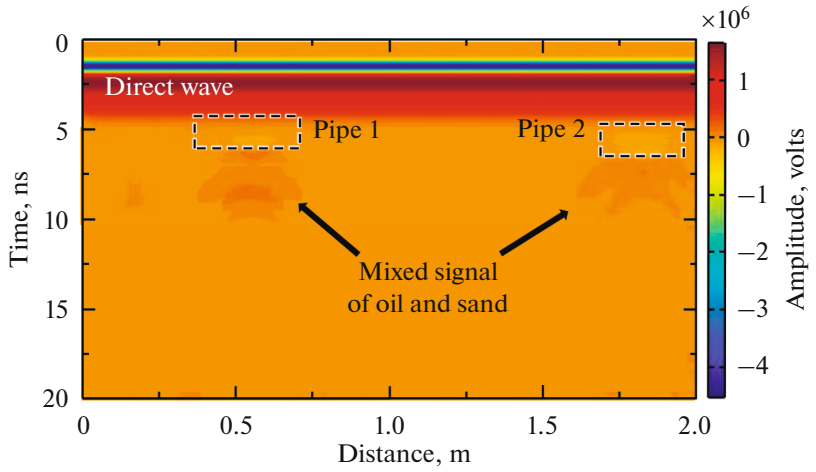

Fig. 12. Cross-sectional view of numerical simulation radar for pipeline filling oil and sand.

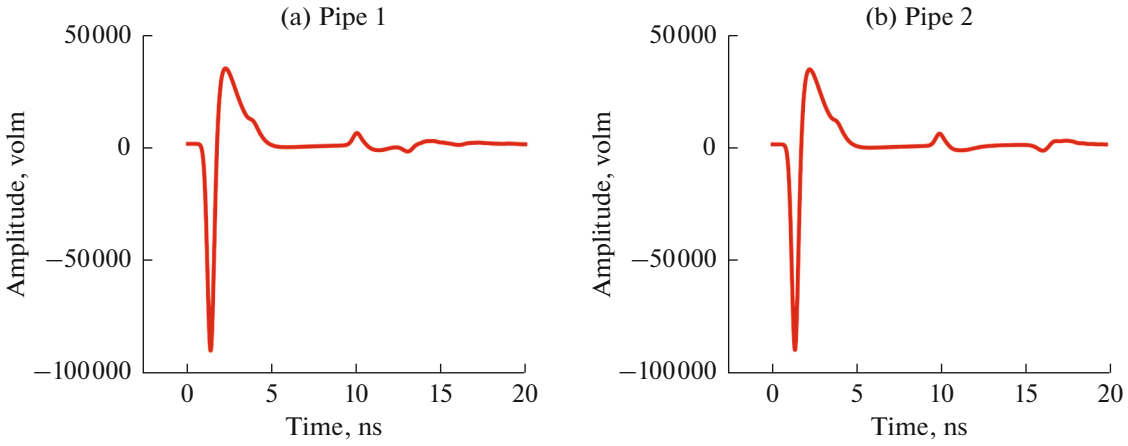

Fig. 13. Single-channel wave of numerical simulation radar for pipeline filling oil and sand.

After pipe 1 and pipe 2 are taken out, the simulation scenario (2) in Figs. 12 and 13 shows similar features to the simulation scenario (1). Three parallel isotropic axis misalignment regions and the lower portion are wider than the upper portion. The reason is that there is a boundary diffraction signal. The oil area is equivalent to a waveform amplifier. The distance between the parallel multiple reflections of the second pipe is large. The electrical difference between the filling medium in the pipe and surrounding medium is larger, the reflection is more obvious and strong. In the single-channel waveform diagram, the pipeline with oil is high-resistance, the first-coming emission wave at the top of the void is opposite to the phase of the incident wave. The first-time reflected wave at the bottom and the reflected wave at the top interfere with each other, it makes the inflection point drown in the signal.

The single channel waveform is shown in Fig. 13. The relative dielectric constant of the pipeline is set small. There are obvious reflection anomalies in the radar profile for both pipes. It depends on the size of pipe, the reflection shows a different performance. There is a diffraction phenomenon of electromagnetic waves at the boundary of pipeline one. This is a concrete manifestation of the electrical difference between the pipeline and surrounding soil. The approximate area of the soil can be judged by the position of boundary diffraction. The electromagnetic wave signal and the diffraction signal of boundary are superimposed at the bottom, the bottom of pipe can be judged by the position of intersection. For the two pipes, the soil signal shows an asymmetrical feature in the profile. There is a certain degree of electromagnetic wave loss in the process of electromagnetic signal propagating from the top to the bottom.

Due to the small extent of the pipeline and the increase in depth compared to pipeline two, the pipeline one only shows a hyperbolic reflection signal with a small curvature on the radar profile, the excitation wave is more excited, the hyperbolic boundary propagates farther on the radar profile. It shows that when the pipeline is gradually reduced to a certain extent, the geological radar loses its ability to judge the scope of the pipeline.

4. CONCLUSIONS

(1) The simulation results show that the layered characteristic signal is a linear signal. The circular pipeline characteristic signal is a hyperbolic in-phase axis signal with the opening facing down. According to the coordinates of the hyperbolic inflection point, the horizontal center position and the upper surface depth of pipeline can be quantitatively estimated, the diameter of pipe and the depth of lower surface are difficult to be directly calculated from the image data.

(2) The different sizes of pipeline cause the different electromagnetic waves angles signal. The radius of curvature hyperbola on the image is larger, when the diameter of pipe is larger. The length of the two ends is larger, the signal is clearer. It is verified that the pipe diameter and vertical depth are proportional to the horizontal length and vertical length of strong reflection signal on the outer surface of signal region respectively.

(3) When the pipeline is filled with oil, the liquid medium is with a high dielectric constant and the hyperbolic interfaces of pipelines are no longer obvious. The strong signal accompanying the oil region shows a hyperbolic contour, it is not clear in-phase axis. The characteristic signal of oil- filled pipeline on the sectional view is a crescent-shaped signal with a downward opening. The area of the reflective area for pipeline is reduced, the absorption of electromagnetic waves is strong, there is no unnecessary diffraction.

FUNDING

Financial support comes from the National Natural Science Foundation of China (Grant no. 51508159), the Fundamental Research Funds for the Central Universities of Hohai University (no. 2019B12914), the Key Laboratory of Ministry of Education for Geomechanics and Embankment Engineering, Hohai University (no. GHXN201904) are gratefully appreciated.

CONFLICT OF INTEREST

The authors declare that they have conflict of interest. The founding sponsors had no role in the design of the study; in the collection, analyses or interpretation of data; in the writing of the manuscript; or in the decision to publish the results.

REFERENCES

1. Jernelöv, A., Environmental effects of terrestrial oil spills, in *Encyclopedia of the Anthropocene*, 2018, pp. 323–335.

2. Xie, P., Wen, H., Xiao, P., and Zhang, Y., Evaluation of ground-penetrating radar (GPR) and geology survey for slope stability study in mantled karst region, *Environ. Earth Sci.,* 2018, vol. 77, p. 122.
3. Gizzi, F.T. and Leucci, G., Global research patterns on ground penetrating radar (GPR), *Surveys Geophys.*, 2018, vol. 2, pp. 1–30.
4. Cataldo, A., Benedetto, E.D., Cannazza, G., Leucci, G., Giorgi, L D., and Demitri, C., Enhancement of leak detection in pipelines through time-domain reflectometry/ground penetrating radar measurements., *IET Sci., Meas. Technol.,* 2017, vol. 11, pp. 696–702.
5. Ocaña-Levario, S.J., Carreño-Alvarado, E.P., Ayala-Cabrera, D., and Izquierdo, J., GPR image analysis to locate water leaks from buried pipes by applying variance filters, *J. Appl. Geophys.,* 2018, vol. 152, pp. 236–247.
6. Amran, T.S.T., Ismail, M.P., Ahmad, M.R., Amin, M.S.M., Ismail, M.A., and Sani, S., Monitoring underground water leakage pattern by ground penetrating radar (GPR) using 800 MHz antenna frequency, *IOP Conf. Ser.: Mater. Sci. Eng.,* 2018, vol. 298, p. 012002.
7. Varughese, A. and Khanna, R., Geophysical investigations using ground penetrating radar (GPR) for hydroelectric projects, *Water & Energy Int.,* 2017, vol. 60, pp. 53–57.
8. PueyoAnchuela, Ó., Frongia, P., Gregorio, F.D., Sainz, A.M.C., and Juan, A.P., Internal characterization of embankment dams using ground penetrating radar (GPR) and thermographic analysis: A case study of the MedauZirimilis Dam (Sardinia, Italy), *Eng. Geol.,* 2018, vol. 237.
9. Chen, Jun, Zhao,Yonghui, and Wan, Minghao, Application of geological radar in underground pipeline detection, *J. Eng. Geophys.,* 2005, vol. 4, p. 260.
10. Ge, R.B. and Qiu, G.X., Using the GPR to detect the diameters of the nonmetallic water pipes, *Urban Geotech. Invest. Surv.,* 2009.
11. Lin, C.J. and Li, S.C., Ground penetrating radar (GPR) and its application in tunnel engineering, *Appl. Mech. Mater.,* 2014, vols. 501–504, pp. 1783–1786.
12. Lalagüe, A., Lebens, M.A., Hoff, I., and Grøv, E., Detection of rockfall on a tunnel concrete lining with ground-penetrating radar (GPR), *Rock Mech. & Rock Eng.,* 2016, vol. 49, pp. 2811–2823.
13. Yanqi, Wu, Liu, S.X., Lei, Fu, and Hongqing, Li, Forward modeling on shallow bridge foundation defect detection by GPR, *Geophys. & Geochem. Explor.,* 2017.
14. Lai, W.W.L., Chang, R.K.W., and Sham, J.F.C., A blind test of nondestructive underground void detection by ground penetrating radar (GPR), *J. Appl. Geophys.,* 2018, vol. 149, pp. 10—17.
15. Yu, Kai, *Signal Processing and Analysis of Ground Penetrating Radar Based on Hilbert-Huang Transform*, Central South Univ., 2010.
16. Zhang, Hui, Liu, Zhenhong, Yang, Qing, Zhao, Zhen, and Sun, Congjun, Application of geological radar to detect groundwater petroleum hydrocarbon pollution in gas stations, *Environ. Eng.,* 2013, vol. S1, pp. 229–232+258.
17. Zhou, Xun, *Study on Leakage Pollution of Underground Storage Tanks in Gas Stations in Southern Jiangsu,* Chinese Acad. Geol. Sci., 2007.
18. Bai, Bing and Zhou, Jian, Development and application status of ground penetrating radar testing technology, *Chin. J. Rock Mech. Eng.,* 2001, vol. 4, pp. 527–531.